Role of ρ^2 term in pion-nucleus dynamics

L. C. Liu

Institute of Nuclear Theory and Department of Physics, Brooklyn College of the City University of New York, Brooklyn, New York 11210

(Received 23 August 1977; revised manuscript received 21 October 1977)

We study the corrections to the first-order optical potential in π-nucleus elastic scattering from 28 to 260 MeV. The dynamical effects of true pion absorption (and correlations) are incorporated into our analysis through the inclusion of a second-order optical potential. We have performed a χ^2 fit to the measured π-^{4}He and π-^{12}C elastic differential cross sections in order to determine a parametrization of the second-order optical potential. It is shown that the inclusion of these higher-order effects not only yields excellent fits to the low-energy data (< 50 MeV), but also systematically improves calculated cross sections at the larger angles in the resonance region. We also find a general improvement in the agreement between the calculated and measured total cross sections, in particular at low energies. Since our first-order potential is essentially parameter free, we believe that the parameters of the second-order potential determined from the present work are meaningful and may serve as a useful guide in future microscopic analyses.

[NUCLEAR REACTIONS Pion-helium and pion-carbon scattering (28–260 MeV). Role of second-order optical potential.]

I. INTRODUCTION

The elastic scattering of charged pions by finite nuclei at low and intermediate energies has been extensively studied in recent years. In several cases, elastic scattering differential cross sections were measured with great accuracy over a large angular range. The availability of such rich experimental information greatly facilitates detailed studies of pion-nucleus dynamics. Various theoretical schemes have been proposed in the literature for the construction of a first-order pion-nucleus optical potential.[1] However, most of theoretical analyses rely heavily on the use of a "fixed-scatterer approximation" (FSA). While modifications of the FSA (for example, the introduction of energy shifts,[2,3]) can lead to good fits to the data, the theoretical uncertainties induced by these modifications lead to difficulties in the study of higher-order corrections, particularly in the resonance region.

In the past we have performed dynamical calculations using the first-order optical potential of a covariant theory.[4] The theory provides a satisfactory account of the differential cross sections over a range of energies.[3,5] At the lower energies ($\lesssim$50 MeV) it is apparent that the inclusion of higher-order effects such as true pion absorption is necessary in order to fit the data. As we will show in this work, extending the consideration of such higher-order effects over the range of energies 30 to 300 MeV provides us with a mechanism for producing excellent fits to all the elastic scattering data. We wish to point out that it is only the careful treatment of Fermi motion and binding effects in the dynamical calculations that makes the present investigation meaningful. The necessity of including true pion absorption in a theory of pion-nucleus interaction has been particularly stressed by Lenz.[6] Recently, we have shown that the inclusion of these effects provides a mechanism for obtaining good agreement with the data for π-^{4}He scattering at 50 MeV.[7] The importance of true pion absorption has since been confirmed by other researchers who have only considered energies less than 100 MeV.[8,9]

In this work we have introduced a phenomenological second-order optical potential [of the form given in Eq. (2.10)]. The parameters which, in the main, measure the strengths of the s-wave and p-wave contributions are determined by performing a χ^2 fit to the differential cross sections. Our results show that the introduction of the second-order optical potential provides an excellent fit to π-^{4}He and π-^{12}C elastic scattering data from 28 to 260 MeV. The energy dependence of the parameters is found to be continuous. Further, in some cases the real and imaginary parts of the parameters appear to be related by a dispersion relation. The general continuity of the p-wave parameters determined in the χ^2 fit is most remarkable in that the χ^2 fit was performed entirely independently of any preconceived theoretical constraints.

Since the wavelength of the pion at energies below 180 MeV is not short enough to probe the short-range nucleon-nucleon correlations, our second-order potential at these lower energies can be mainly ascribed to the dynamics of true pion absorption. At pion energies between 180 and 300 MeV, the scattering of pions by correlated nucle-

ons may become important. However, owing to the large cross section for pion absorption in the resonance region,[6,10] the role of correlations is unlikely to be predominant. The unfolding of correlation effects from true pion absorption effects at higher energies deserve further theoretical study and is currently under investigation. For simplicity, in the following we will assume that the second-order potential introduced in this work represents the effects of true pion absorption, keeping in mind that the effects of short-range correlations are also present in our phenomenological form.

We will present in the next section the basic formulas as well as the parametrization of second-order optical potential used for the calculation. Our main results will then be discussed in Sec. III. [The readers who are mainly interested in the results of our analysis may survey the figures and tables after the inspection of Eq. (2.10).]

As we shall see, the inclusion of a ρ^2 term in the optical potential not only improves the large angle differential cross sections at all energies, but also leads to systematic agreement between the theoretical results and the data on total cross sections. We believe that the results of our phenomenological analysis will provide further stimulus for the construction of microscopic models for the underlying pion-nucleus dynamics.

II. BASIC THEORY

In momentum space the pion-nucleus scattering amplitude satisfies the following *covariant* three-dimensional integral equation:

$$\langle \vec{k}' | \bar{M}(w) | \vec{k} \rangle = \langle \vec{k}' | \bar{K}(w) | \vec{k} \rangle + \int d\vec{k}'' \frac{\langle \vec{k}' | \bar{K}(w) | \vec{k}'' \rangle R(\vec{k}'') \langle \vec{k}'' | \bar{M}(w) | \vec{k} \rangle}{(\vec{k}_0^{\,2} - \vec{k}''^2)/2\mu_{\vec{k}_0} + i\epsilon} . \tag{2.1}$$

Here $\bar{M}$ is the invariant scattering amplitude and $\bar{K}$ is the covariant potential. If we denote the Coulomb interaction by K_C, we may write the total interaction as

$$\bar{K} = K_C + K_N^{(1)} + K_N^{(2)} \tag{2.2}$$

with $K_N^{(1)}$ and $K_N^{(2)}$ representing the first- and second-order covariant optical potentials, respectively. The $K_N^{(1)}$ term has been discussed extensively in the past. The $K_N^{(2)}$ term represents the interaction of the pion with a *pair* of nucleons.

In Eq. (2.1), the quantity w is related to the total energy of the pion-nucleus system by the relation:

$$2w = (\vec{k}_0^{\,2} + M_\pi^{\,2})^{1/2} + (\vec{k}_0^{\,2} + M_A^{\,2})^{1/2} = E_\pi(\vec{k}_0) + E_A(\vec{k}_0) , \tag{2.3}$$

where $\vec{k}_0$ is the pion beam momentum in the π-nucleus c.m. frame. The relativistic phase-space factor R depends on the specific reduction scheme employed in reducing a four-dimensional integral equation to a *covariant* three-dimensional equation. In this work, we use a reduction scheme similar to the one based upon the propagator g_2 of Ref. 11. For the scattering of pions by a spin zero target nucleus, we use the propagator given by

$$G(k'') = \frac{\delta(k''^0 - w + E_A(\vec{k}''))}{(\vec{k}_0^{\,2} - \vec{k}''^2)/2\mu_{\vec{k}_0} + i\epsilon} \frac{(\mu_{\vec{k}''}/\mu_{\vec{k}_0})}{2E_\pi(\vec{k}'')2E_A(\vec{k}'')} , \tag{2.4}$$

where $\mu_{\vec{k}_0} = E_\pi(\vec{k}_0)E_A(\vec{k}_0)/[E_\pi(\vec{k}_0) + E_A(\vec{k}_0)]$. This choice of reduction scheme allows for a consistent treatment of the Coulomb interaction. (The use of a Green's function, of the form $G(k'') = [E_\pi(\vec{k}_0) + E_A(\vec{k}_0) - E_\pi(\vec{k}'') - E_A(\vec{k}'') + i\epsilon]^{-1}$, is inconsistent with the use of standard Coulomb coordinate space wave functions.) We define

$$R(\vec{k}'') = [2E_\pi(\vec{k}'')2E_A(\vec{k}'')]^{-1}(\mu_{\vec{k}''}/\mu_{\vec{k}_0}) \tag{2.5}$$

and rewrite Eq. (2.1) in a more familiar form,

$$\langle \vec{k}' | T(w) | \vec{k} \rangle = \langle \vec{k}' | V(w) | \vec{k} \rangle + \int d\vec{k}'' \frac{\langle \vec{k}' | V(w) | \vec{k}'' \rangle \langle \vec{k}'' | T(w) | \vec{k} \rangle}{\vec{k}_0^{\,2}/2\mu_{\vec{k}_0} - \vec{k}''^2/2\mu_{\vec{k}_0} + i\epsilon} \tag{2.6}$$

by using the definitions:

$$\langle \vec{k}' | T(w) | \vec{k} \rangle \equiv R^{1/2}(\vec{k}') \langle \vec{k}' | \bar{M}(w) | \vec{k} \rangle R^{1/2}(\vec{k}) \tag{2.7}$$

and

$$\langle \vec{k}' | V(w) | \vec{k} \rangle \equiv R^{1/2}(\vec{k}') \langle \vec{k}' | \bar{K}(w) | \vec{k} \rangle R^{1/2}(\vec{k}) . \tag{2.8}$$

It is clear that the T and V in the above equations can be identified with the usual Schrödinger equation T matrix and V matrix in the low-energy limit. Our expression for the first-order optical potential is given by

$$\langle \vec{k}' | V_N^{(1)}(w) | \vec{k} \rangle = \sum_{njls's''} \int d\vec{Q} R^{1/2}(\vec{k}') [M_{nlj}/E_{nlj}(\vec{Q})] \bar{u}^{s''}(P' - Q) [(2\pi)^3 \langle p', P' - Q | M_{\pi N}(s) | p, P - Q \rangle] u^{s'}(P - Q) \cdot \times F_{s's''}^{n(j\frac{1}{2})l}(\vec{Q}_R, \vec{Q}_R') R^{1/2}(\vec{k}) . \tag{2.9}$$

In Eq. (2.9) the quantities $\bar{u}M_{\pi N}\,u$ and F are, respectively, the invariant (off-shell) π-N amplitude and the invariant nuclear density matrix. The letters (njl) specify the hole state in the spectator nucleus. This

spectator nucleus has momentum $\vec{Q}$ and mass M_{nj}. Further, $\vec{Q}_R$ and $\vec{Q}'_R$ denote the momenta of the struck nucleon in the rest frame of the target nucleus of mass M_A. The nuclear binding and the Fermi motion of the struck nucleon affects the π-N amplitude mainly in the determination of s, the square of the invariant mass of the π-N system. [We refer to Refs. 3 and 7 for a detailed discussion of the consequences of our determination of the values of s. Note that $s=(p+P-Q)^2=(p'+P'-Q)^2$.]

We parametrized the second-order optical potential in the following way:

$$\langle \vec{k}' | V_N^{(2)}(w) | \vec{k} \rangle = R^{1/2}(\vec{k}')(2M_A)A(A-1)(2\pi)^3\left(\int e^{-i(\vec{k}-\vec{k}')\cdot\vec{r}}[\rho(\vec{r})]^2 d\vec{r}\right)$$

$$\times\left(B(k_0)\frac{v_0(k')v_0(k)}{[v_0(k_0)]^2}+k_0^2C(k_0)\hat{k}'\cdot\hat{k}\frac{v_1(k')v_1(k)}{[v_1(k_0)]^2}\right)R^{1/2}(\vec{k}) \tag{2.10}$$

with

$$v_0(k)=\frac{C_0}{\vec{k}^2+\alpha_0^2} \tag{2.11}$$

and

$$v_1(k)=\frac{C_1 k}{\vec{k}^2+\alpha_1^2}\ . \tag{2.12}$$

Here B and C are energy-dependent complex parameters which represent, in the main, the s- and p-wave π-nucleus absorption strength. The v_0 and v_1 are the "form factors" for s and p waves π-*nucleus* interactions. (In general the fundamental absorption amplitudes classified according to their angular momentum are mixed together when these amplitudes are transformed into the c.m. frame of the π-nucleus system. Because of this, we do not make a precise identification of the form factors v_0 and v_1, but consider them as part of our phenomenological specification. Further theoretical study of the second-order optical potential should provide a better understanding of the nature of our phenomenological potential and of the physical signigicance of v_0 and v_1.)

In the zero-range limit ($\alpha_i \to \infty$), we have the more conventional forms:

$$B(k_0)\frac{v_0(k')v_0(k)}{[v_0(k_0)]^2}\to B(k_0) \tag{2.13}$$

and

$$k_0^2C(k_0)\hat{k}'\cdot\hat{k}\frac{v_1(k')v_1(k)}{[v_1(k_0)]^2}\to\vec{k}'\cdot\vec{k}C(k_0)\ . \tag{2.14}$$

It is then possible to relate the parameters B and C to the absorption parameters B_0 and C_0 employed by Tauscher and Schneider in their coordinate space analysis of the pionic-atom optical potential.[12] We find

$$B=B_0\left(\frac{A}{A-1}\right)(16\pi^5)^{-1}(1+M_\pi/2M_N) \tag{2.15}$$

and a similar relation between C and C_0. The factor $(16\pi^5)^{-1}$ is due to the different normalization factor for the plane wave states employed in this work and in Ref. 12, while the factor $A/(A-1)$ arises from the fact we have employed the actual number of nucleon pairs, $A(A-1)/2$, in our potential $V_N^{(2)}$ in lieu of the usual A^2 factor. [It is interesting to note that the use of the $A(A-1)$ factor removes the anomaly in the value of B_0 obtained in the pionic-atom analysis in the case of ^{4}He.[12]]

III. RESULTS AND DISCUSSIONS

We have performed a χ^2 fit to the data by varying the two complex parameters B and C defined in Eq. (2.10). In one case, the fit was carried out with $\alpha_i=\infty$ (the zero-range limit); in the other case, we have used $\alpha_i=700$ MeV/c. Such calculations have been made for π^--^{4}He scattering at 51, 110, 150, 180, 220, and 260 MeV. The 51 MeV data are due to Crowe *et al.*[13]; the other data are from Binon *et al.*[14] We have also made a χ^2 fit to the π^+-^{12}C data at 28 and 49 MeV,[8,15] and to the π^--^{12}C data at 120, 150, 180, 230, and 260 MeV.[16] For the basic π-N amplitudes used in the calculation of the first-order optical potential, we have used the CERN-TH phase shifts[17] and the LMM off-shell model.[18] However, we have modified the CERN-TH phase shifts at low energies so as to insure the correct threshold behavior. This modification makes our low-energy phase shifts very close to those given by Salomon.[19]

The theoretical differential cross sections calculated without and with the inclusion of the second-order potential for the case $\alpha_1=\alpha_2\equiv\alpha=\infty$ are compared with the data in Figs. 1–9. (The theoretical cross sections calculated with the inclusion of $V_N^{(2)}$ for $\alpha=700$ MeV/c are very similar to those cross sections obtained for $\alpha=\infty$.) One may see from these figures that the effect of adding $V_N^{(2)}$ to the optical potential significantly improves the theoretical results. At lower energies ($T_\pi<50$ MeV), the inclusion of $V_N^{(2)}$ improves the results especially in the angular region where there is a minimum in the measured cross sections. At higher

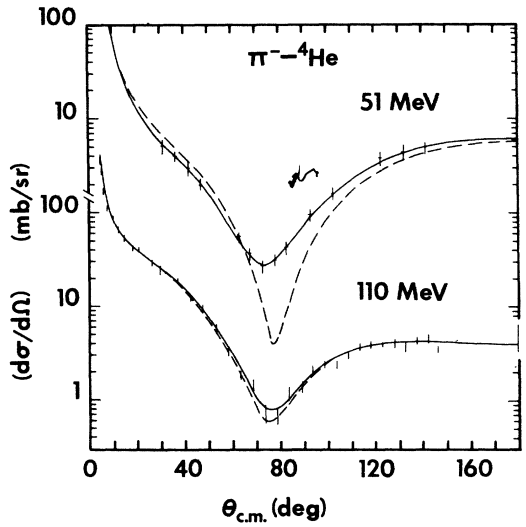

FIG. 1. Comparison of the data (Ref. 14) for π^--^{4}He elastic scattering at 51 and 110 MeV with various theoretical calculations. The dashed curves result from the use of $V_c + V_N^{(1)}$ only. The solid curves include the potential $V_N^{(2)}$ in the zero-range limit ($\alpha = \infty$). (The curves corresponding to a finite range calculation with $\alpha = 700$ MeV/c are very similar to the solid curves shown in the figure).

energies, the effect of $V_N^{(2)}$ is to significantly improve the calculated cross sections at the larger angles. These features can be understood easily. The potential $V_N^{(2)}$ depends on the square of the

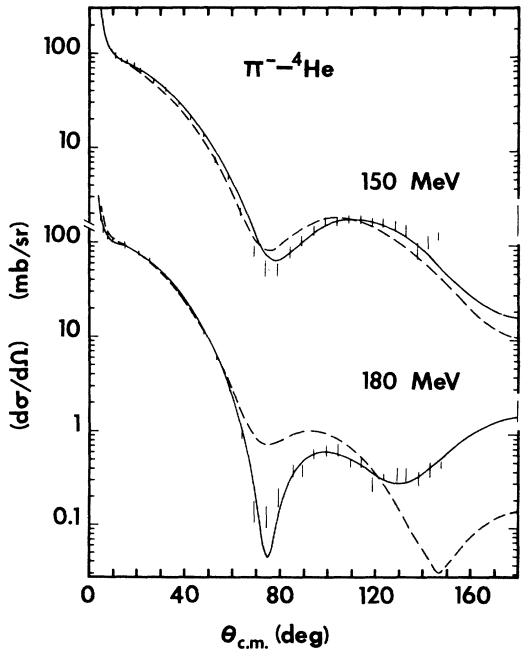

FIG. 2. Same caption as Fig. 1 with $T_\pi = 150$ and 180 MeV.

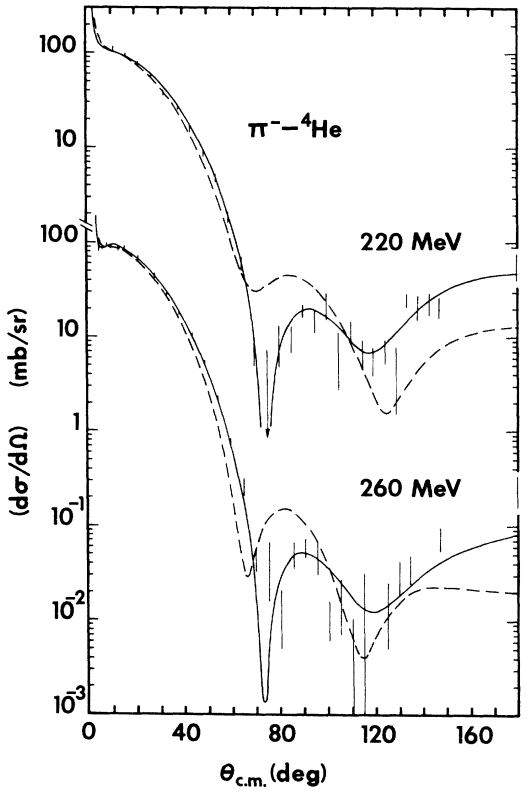

FIG. 3. Same caption as Fig. 1 with $T_\pi = 220$ MeV and 260 MeV.

nuclear density. For light nuclei, such as ^{4}He and ^{12}C, the square of the nuclear density is a more rapidly decreasing function of r, the distance from the center of the nucleus, than the nuclear density itself. Consequently, *the inclusion of $V_N^{(2)}$ mainly alters the π-nucleus interaction strength in the central region. The interaction in the peripheral region is still dominated by $V_N^{(1)}$.* We remark that in the resonance region the potentials $V_N^{(1)}$ and $V_N^{(2)}$ are highly absorptive. Thus the differential cross sections are mainly sensitive to the details of the interaction in the surface. In the regions of smallest density this interaction is dominated by $V_N^{(1)}$ but as one moves further toward the center of the nucleus $V_N^{(1)}$ and $V_N^{(2)}$ become comparable in magnitude. The subtleties of this radial dependence leads to interesting effects. For example, the cross section at forward angles is rather insensitive to the magnitude of $V_N^{(2)}$ while the cross section at the larger angles is very sensitive to this quantity. These features may be observed in the figures representing the cross sections in the resonance region.

In Table I we present the values of the complex parameters B and $k_0^2 C$ determined for π-^{4}He scattering. The constants are given for the zero-range

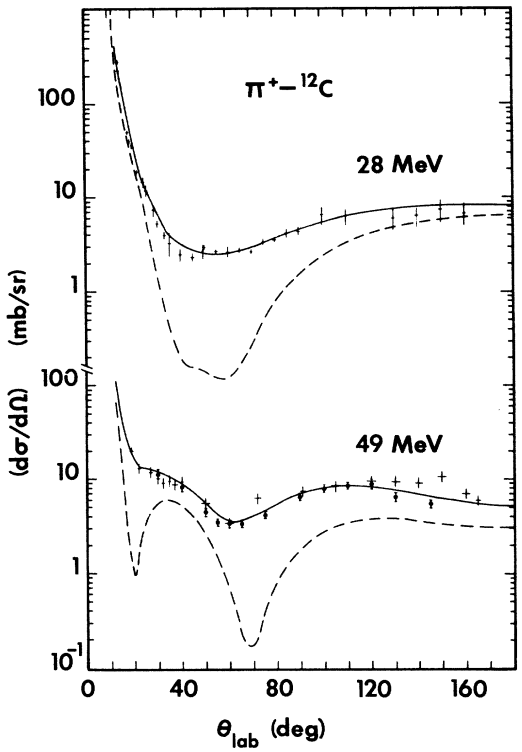

FIG. 4. Comparison of the data for π^+-^{12}C elastic scattering at 28.4 and 48.9 MeV with various theoretical calculations. The data marked by (+) and by (Φ) are taken from Refs. 8 and 15, respectively. The curves have the same meanings as in Fig. 1.

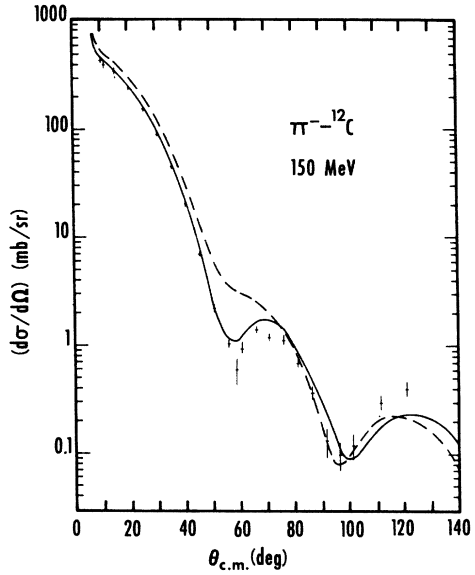

FIG. 6. Same caption as Fig. 5 with $T_\pi = 150$ MeV.

case ($\alpha = \infty$) and for the finite range case ($\alpha = 700$ MeV/c). In the zero-range case the corresponding values of B_0 and C_0 are also presented, making use of Eq. (2.15). The values of the complex parameters B and k_0^2C for π-^{12}C scattering are presented in Table II. The real and imaginary parts of B and k_0^2C which are functions of the pion energy are shown in Figs. 10–15. The continuous curves are drawn as a guide to the eye. In the resonance re-

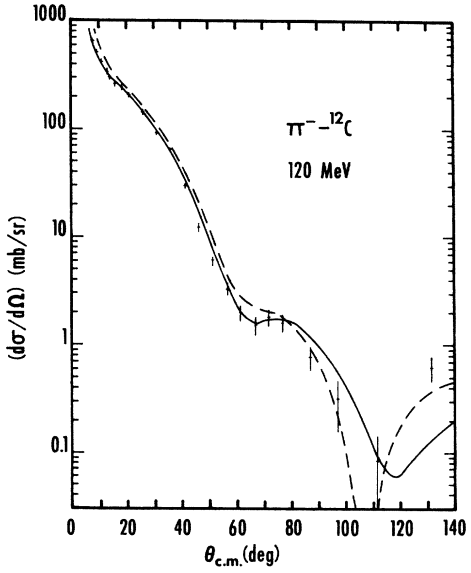

FIG. 5. Comparison of the data (Ref. 16) for π^--^{12}C elastic scattering at 120 MeV with various theoretical calculations. The curves have the same meanings as in Fig. 1.

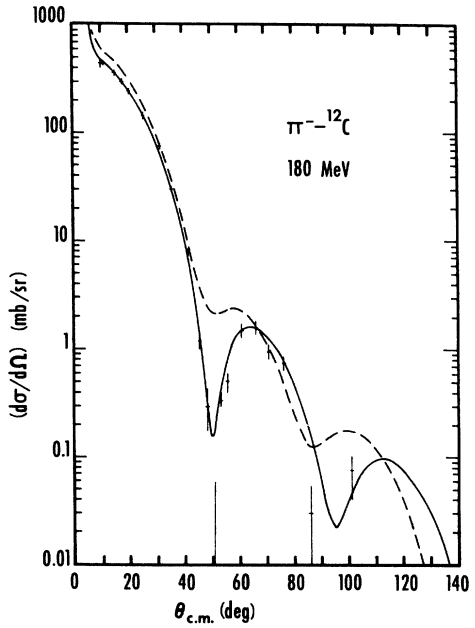

FIG. 7. Same caption as Fig. 5 with $T_\pi = 180$ MeV.

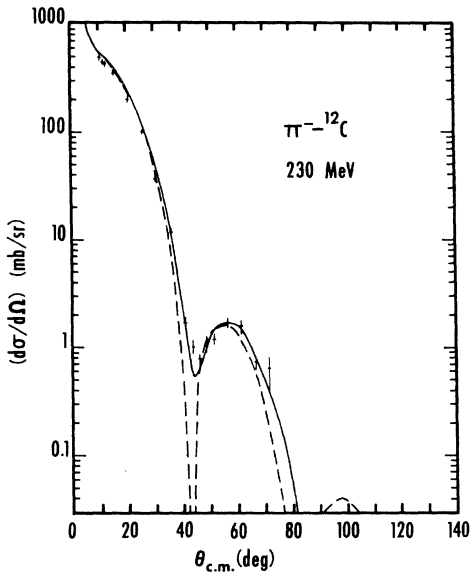

FIG. 8. Same caption as Fig. 5 with $T_\pi = 230$ MeV.

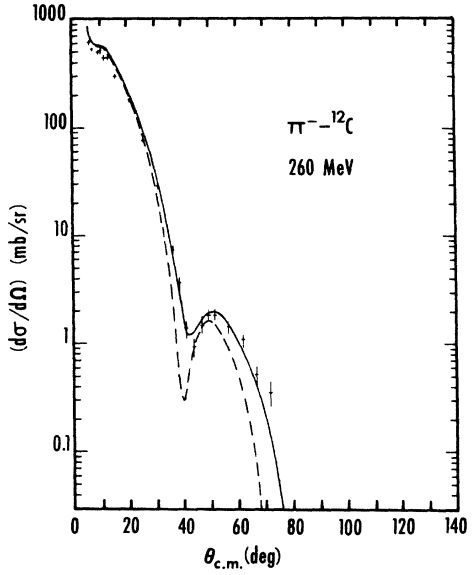

FIG. 9. Same caption as Fig. 5 with $T_\pi = 260$ MeV.

gion, the real and imaginary parts of the p-wave parameter, k_0^2C, exhibit dispersion-like behavior. *It is important to note that above* 110 MeV *the p-wave parameters are an order of magnitude greater than the s-wave parameters.* To show this aspect more clearly, we present in Fig. 16 the magnitudes of the ImB, Imk_0^2C, and Im$(B + k_0^2C)$ for the zero-range case and for π-^{4}He scattering. The curves for carbon are similar to those of Fig. 16. Upon inspecting the figures, one may also infer that the true pion absorption contribution may become relatively unimportant at pion energies above 400 MeV. Further, we remark from Tables I and II that the constant C_0 vanishes as T_π goes to zero. The values of B_0 determined from our work take the form $B_0 = |b| - i|b|$ at low energies ($T_\pi < 50$ MeV). (This form was suggested by Tauscher and Schneider[12] in their analysis of pionic atoms.)

If one restores the various factors relating $B(k_0) + k_0^2C(k_0)$ to the matrix element of the potential, $V_N^{(2)}$ [see Eq. (2.10)], one finds that the potentials for ^{4}He and ^{12}C are not very different at low energies. We hope to study π-^{16}O elastic scattering using the same method, since we expect the parameters for ^{16}O should be similar to those for ^{12}C. As we investigate systems with large mass num-

TABLE I. Values of the s- and p-wave parameters of $V_N^{(2)}$ for π-^{4}He scattering.

			$\alpha = \infty$			$\alpha = 700$ MeV/c	
T_π (MeV)	k_0 (fm^{-1})	B_0 (M_π^{-4})	C_0 (M_π^{-6})	B (fm^4)	k_0^2C (fm^4)	B (fm^4)	k_0^2C (fm^4)
51	0.6260	+0.091	+0.0	+1.05(−4)	+0.0	+1.09(−4)	+0.0
		−i0.096	−i0.0	−i1.12(−4)	−i0.0	−i1.07(−4)	−i0.0
110	0.9842	+0.028	−0.038	+3.36(−5)	−8.60(−5)	+3.91(−5)	−7.94(−5)
		−i0.013	−i0.064	−i1.46(−5)	−i1.45(−4)	−i1.46(−5)	−i1.24(−4)
150	1.196	−0.079	−0.197	−9.97(−5)	−7.09(−4)	−1.16(−5)	−1.03(−4)
		−i0.003	−i0.092	−i3.64(−6)	−i3.32(−4)	−i1.50(−6)	−i1.80(−4)
180	1.345	−1.33	−1.92	−1.56(−3)	−8.12(−3)	−5.45(−4)	−5.77(−4)
		−i0.27	−i2.50	−i3.19(−4)	−i1.06(−2)	−i4.30(−4)	−i6.22(−3)
220	1.537	+0.40	+0.94	+4.68(−4)	+5.20(−3)	−2.40(−4)	+3.92(−3)
		−i0.22	−i1.57	−i2.51(−4)	−i8.65(−3)	−i3.19(−4)	−i3.38(−3)
260	1.721	+0.25	+0.37	+2.89(−4)	+2.54(−3)	+2.20(−4)	+1.69(−3)
		−i0.026	−i0.026	−i2.98(−5)	−i1.76(−4)	−i1.60(−5)	−i9.48(−5)

TABLE II. Values of the s- and p-wave parameters of V_N for π-^{12}C scattering.

				$\alpha=\infty$		$\alpha=700$ MeV/c	
T_π (MeV)	k_0 (fm^{-1})	B_0 (M_π^{-4})	C_0 (M_π^{-6})	B (fm^4)	k_0^2C (fm^4)	B (fm^4)	k_0^2C (fm^4)
28.4	0.4667	+0.16	−0.048	+1.55(−4)	−2.01(−5)	+1.50(−4)	−1.85(−5)
		$-i$0.097	$-i$0.0	$-i$9.35(−5)	$-i$0.0	$-i$8.98(−5)	$-i$0.0
48.9	0.6313	+0.21	−0.16	+1.98(−4)	−1.25(−4)	+1.90(−4)	−1.19(−4)
		$-i$0.0	$-i$0.16	$-i$0.0	$-i$1.21(−4)	$-i$9.12(−7)	$-i$1.24(−4)
120	1.084	−0.13	−0.25	−1.20(−4)	−5.63(−4)	−2.46(−4)	−2.26(−4)
		$-i$0.013	$-i$0.63	$-i$1.20(−5)	$-i$1.41(−3)	$-i$7.80(−6)	$-i$1.43(−3)
150	1.254	−0.083	−0.31	−7.95(−5)	−9.26(−4)	−2.74(−4)	+4.62(−4)
		$-i$0.014	$-i$0.79	$-i$1.35(−5)	$-i$2.36(−3)	$-i$4.89(−5)	$-i$2.33(−3)
180	1.417	−0.052	+0.43	−4.94(−5)	+1.65(−3)	−2.39(−4)	+2.03(−3)
		$-i$0.020	$-i$0.63	$-i$1.95(−5)	$-i$2.43(−3)	$-i$2.61(−5)	$-i$2.45(−3)
230	1.680	+0.148	+0.48	+2.06(−4)	+2.61(−3)	+7.71(−5)	+2.39(−3)
		$-i$0.002	$-i$0.067	$-i$1.80(−6)	$-i$3.61(−4)	$-i$1.80(−5)	$-i$3.61(−4)
260	1.833	+0.017	+0.32	+1.61(−5)	+2.07(−3)	+3.01(−5)	+1.56(−3)
		$-i$0.008	$-i$0.015	$-i$7.55(−6)	$-i$9.68(−5)	$-i$1.31(−5)	$-i$1.31(−4)

ber, we expect we will be able to achieve a more universal parametrization.

The theoretical cross sections, σ_T, σ_{el}, and $\sigma_r \equiv \sigma_T - \sigma_{el}$, calculated for π-^{4}He and π-^{12}C scattering are presented in Tables III and IV, respectively. The comparison between the theoretical total cross sections (obtained with and without $V_N^{(2)}$) and the data is shown in Fig. 17. We see that in general, the inclusion of $V_N^{(2)}$ considerably improves the theoretical results, especially at low energies. Very good agreement with the measured values for σ_T is obtained in most cases. Finally, in Fig. 18 we present the comparison between the real parts of the forward nuclear scattering amplitude calcu-

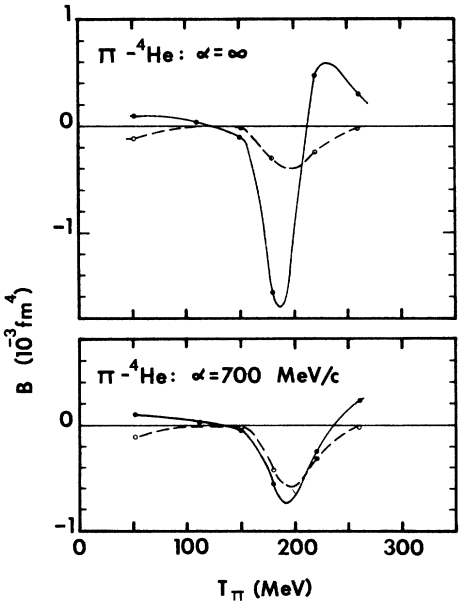

FIG. 10. Real (●) and imaginary (○) parts of the parameter B for π-^{4}He scattering. The curves are drawn only as a guide for the eye.

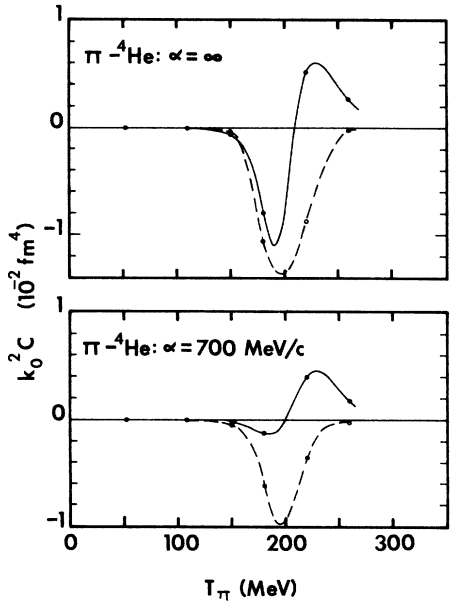

FIG. 11. Real (●) and imaginary (○) parts of the parameter k_0^2C for π-^{4}He scattering. Same caption as for Fig. 10.

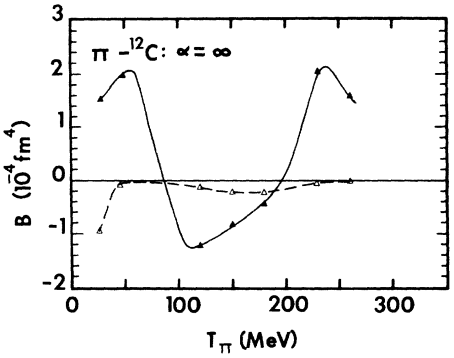

FIG. 12. Real (●) and imaginary (○) parts of the parameter B for π-^{12}C scattering in the zero-range limit ($\alpha = \infty$). The curves are drawn only as a guide for the eye.

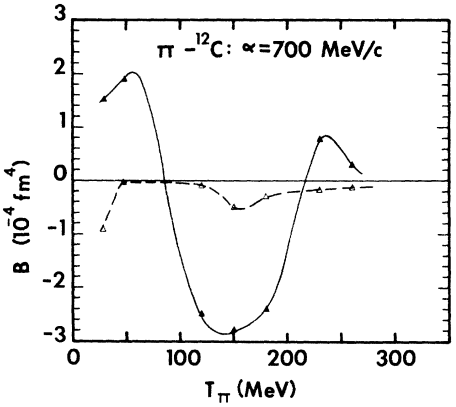

FIG. 14. Same captions as those of Fig. 12 with α = 700 MeV/c.

lated with and without the inclusion of $V_N^{(2)}$. We stress that in the χ^2 fit we have performed, only the experimental elastic differential cross sections were used. The experimental total cross sections have not been used in making the χ^2 fit. Further, we have not required that the parameters of the second-order potential have any smooth energy dependence, that is to say, we have made an energy-independent fit. For these reasons, it is remarkable that our fit yields good agreement with measured total cross sections, a smooth energy dependence of $\mathrm{Re}f_N(0)$, and generally continuous energy dependence of the p-wave parameters. The behavior of the s-wave parameters B in the case of ^{12}C (see Figs. 12 and 14) is not easy to interpret and requires further study. We may conjecture that the oscillations observed in the s-wave pion-*nucleus* parameters are due to "interference effects" obtained when expressing the fundamental absorption amplitudes ($\pi NN \to NN$) in the pion-*nucleus* center of mass frame.

We note that in the case of ^{4}He the data are sufficiently precise so that the parameters B and k_0^2C are very well determined. Our analysis indicates that there are no other solutions which will significantly reduce the value of χ^2. The very large ratio of $|\mathrm{Im}k_0^2C|/|\mathrm{Im}B|$ at 110 MeV (see Fig. 16) makes the value of χ^2 relatively insensitive to variations of the parameter $|\mathrm{Im}B|$ by a factor of 2. However, for the other cases, the parameters are determined to within 10%.

A word of caution is in order, however. As may be seen from the figures, at 110 MeV and above, the π-*nucleus* p-wave absorption is very much larger than the π-*nucleus* s-wave absorption. Thus we have much more confidence that we may ultimately understand these p-wave parameters on the

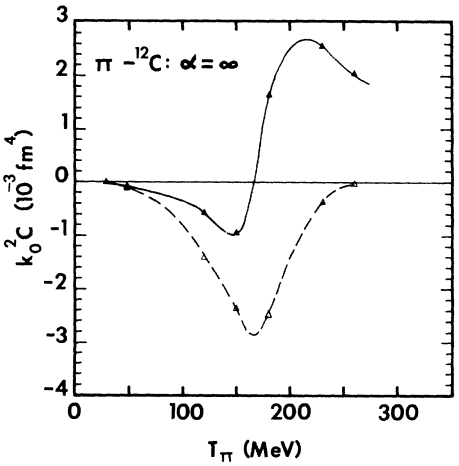

FIG. 13. Real (●) and imaginary (○) parts of the parameter k_0^2C for π-^{12}C scattering in the zero-range limit ($\alpha = \infty$). The curves are drawn only as a guide for the eye.

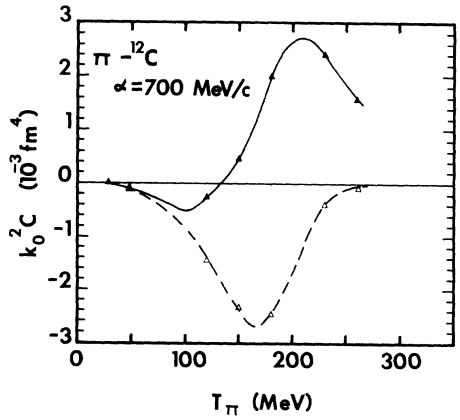

FIG. 15. Same captions as those of Fig. 13 with α = 700 MeV/c.

TABLE III. Calculated cross sections for π-^{4}He scattering.

	Without $V_N^{(2)}$			With $V_N^{(2)}$ ($\alpha=\infty$)			With $V_N^{(2)}$ ($\alpha=700$ MeV/c)		
T_π (MeV)	σ_T (mb)	σ_{el} (mb)	σ_r (mb)	σ_T (mb)	σ_{el} (mb)	σ_r (mb)	σ_T (mb)	σ_{el} (mb)	σ_r (mb)
51	39.9	28.2	11.7	59.6	30.2	29.4	60.9	30.4	30.5
110	168.5	80.4	88.1	197.8	79.6	118.2	201.0	82.5	118.5
150	265.5	102.5	163.0	302.7	112.9	189.8	283.6	111.0	172.2
180	303.3	109.7	193.6	309.9	110.8	199.1	305.5	112.1	193.4
220	282.7	97.1	185.6	271.2	107.9	163.3	269.2	102.4	166.8
260	228.7	76.1	152.5	219.5	83.4	136.1	222.6	85.0	137.6

basis of a microscopic theory.[20] It is possible that some still higher-order effects (for example, ρ^3 terms of the optical potential) are incorporated in the effective small s-wave ρ^2 potential at the higher energies. The somewhat unusual behavior of the s-wave parameters for π-^{12}C scattering (see Figs. 12 and 14) mentioned previously may be an indication of the possible role of still higher-order effects. On the other hand, at 50 MeV we believe the s-wave parameters are well determined and physically significant.

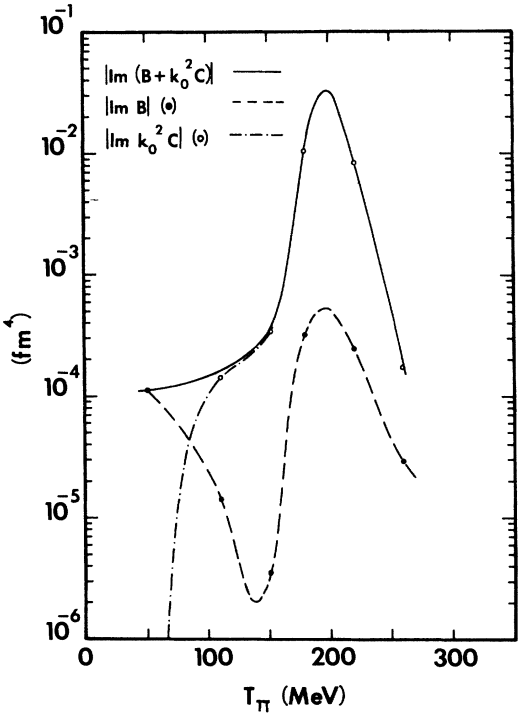

FIG. 16. The magnitudes of the parameters ImB, Imk_0^2C, and Im$(B+k_0^2C)$ for π-^{4}He scattering with $\alpha=\infty$. The curves are drawn only as a guide for the eye.

IV. CONCLUDING REMARKS

We have demonstrated that the second-order optical potential plays an important role in pion-nucleus scattering from 28 to 260 MeV, the energy range we have studied. At low energies, the effects on the cross sections are dramatic over the full range of scattering angles. In the resonance region, the imaginary part of the second-order potential reaches a maximum. [This feature is probably related to the resonance in the ($\pi NN \to NN$) amplitudes.] However, since the first-order optical potential is already very absorptive in the resonance region, the effects of the second-order optical potential can only be seen in the differential cross section at the larger scattering angles.

We would like to identify the true pion absorption mechanism as the main source of our second-order optical potential. This identification can only be made on the basis of further analysis, since we

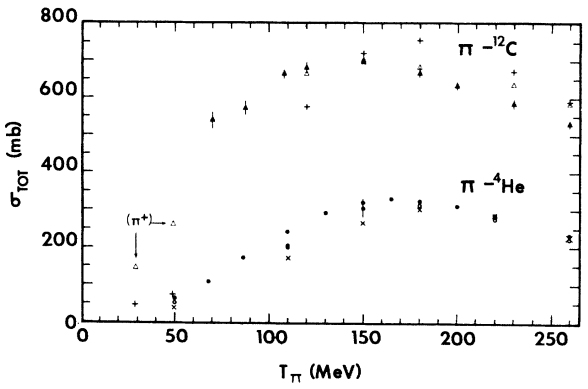

FIG. 17. Comparison of the data (Refs. 14 and 16) for π-^{12}C total cross sections (▲) and π-^{4}He total cross sections (●) with calculated total cross sections. The open triangles and circles represent calculated results including the effects of $V_N^{(2)}$(^{12}C: △; ^{4}He: ○). The (+) and (×) points denote calculated results in the absence of second-order effects (^{12}C: +; ^{4}He: ×).

TABLE IV. Calculated cross sections for π-^{12}C scattering.

	Without $V_N^{(2)}$			With $V_N^{(2)}$ ($\alpha=\infty$)			With $V_N^{(2)}$ ($\alpha=700$ MeV/c)		
T_π (MeV)	σ_T (mb)	σ_{el} (mb)	σ_r (mb)	σ_T (mb)	σ_{el} (mb)	σ_r (mb)	σ_T (mb)	σ_{el} (mb)	σ_r (mb)
28.4	46.0	27.6	18.4	142.1	74.8	67.3	142.1	74.9	67.2
48.9	71.4	42.2	29.2	260.9	101.6	159.3	259.6	101.9	157.7
120	576.6	311.0	265.6	664.7	238.6	426.1	664.3	240.7	423.6
150	717.3	341.8	375.5	714.6	267.4	447.2	703.0	253.2	449.8
180	752.8	314.0	438.8	680.4	249.5	430.9	678.6	249.6	429.0
230	673.2	254.2	419.0	637.3	255.5	381.8	648.0	262.9	385.1
260	588.7	223.8	364.9	582.7	248.9	333.7	588.7	249.4	339.3

have not fully excluded the possibility that short-range and other nucleon-nucleon correlations contribute in an important manner to the second-order potential in the resonance region. We have seen, however, in a previous study[21] that the highly off-shell nature of the scattering of a pion from a correlated pair of nucleons is quite important. It is *only* in the FSA that one would expect resonant effects at $T_\pi \simeq 180$ MeV in the scattering of a pion from a correlated pair. In a fully dynamical theory the analysis of such amplitudes is rather complicated. We believe that most resonant effects in such amplitudes would be suppressed by off-shell effects. In lieu of a fully microscopic theoretical analysis, we suggest that a study of the total pion absorption cross section will be necessary for clarifying this situation.

One may also inquire as to the importance of pion absorption in the π-*nucleus d* wave. We have found no evidence for such a mechanism at energies $T_\pi \leq 180$ MeV. At 220–260 MeV, the large

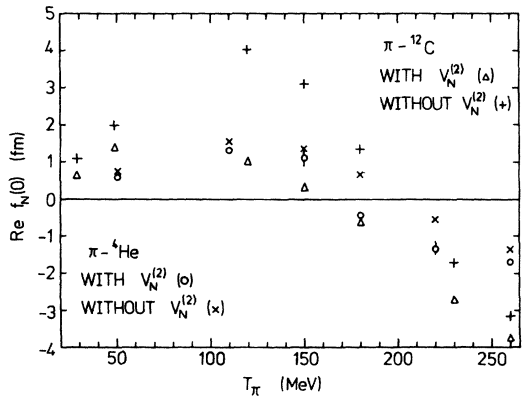

FIG. 18. Energy dependence of Re$f_N(0)$. The (Δ) and (+) points, respectively, correspond to π-^{12}C scattering amplitude with and without the inclusion of $V_N^{(2)}$. The (○) and (×) points, respectively, correspond to the π-^{4}He scattering amplitude with and without the inclusion of $V_N^{(2)}$.

error bars for the differential cross sections at large angles in π-^{4}He scattering and the absence of data for $\theta_{c.m.} > 90°$ for π-^{12}C elastic scattering do not allow us to make definite conclusions.

Finally, we remark that the analysis we have carried out is only made possible by the existence of very high quality data at several energies. We suggest that in future experiments an attempt be made to achieve data of similar accuracy.

ACKNOWLEDGMENTS

This work is supported in part by the PSC-BHE Research Award Program of the City University of New York. The author wishes to thank Professor C. M. Shakin for discussions on various aspects of this work.

APPENDIX

In our dynamical calculations, we do not use the FSA. Further, we deal with the nuclear density matrix rather than using only the matter density (as in the FSA). The method of obtaining the wave functions needed for constructing the density matrix of ^{4}He from the knowledge of the experimental charge form factor was given in Ref. 5. For ^{12}C, we employed the following procedure. We assume harmonic oscillator shell model wave functions for the s- and p-shell nucleons. We calculate, using these wave functions, the matter form factor $F_{mat}(\vec{q})$ and the charge form factor $F_{ch}(\vec{q}) = F_{mat}(\vec{q})F_{pr}(\vec{q})$. We adjust the harmonic oscillator (HO) parameters of the wave functions to fit the experimental $F_{ch}(\vec{q})$. We use a realistic proton form factor[22] in our calculations. Further, we obtained a better fit to the high momentum part of the charge form factor by allowing the p-shell HO parameter to be slightly different from the s-shell HO parameter. The s- and p-shell wave functions obtained in this manner are given by

$$\varphi_{l=0}(\vec{r}) = \frac{1}{\pi^{3/4} R_0^{3/2}} e^{-r^2/2R_0^2} \tag{A1}$$

and

$$\varphi_{l=1,m}(\vec{r}) = \frac{1}{\pi^{3/4}R_1^{3/2}} (\tfrac{1}{3}8\pi)^{1/2} (r/R_1) e^{-r^2/2R_1^2} Y_{1m}(\hat{r}) \ . \tag{A2}$$

We now comment on the structure of the second-order optical potential. The matrix elements of $V_N^{(2)}$ are given in Eq. (2.10). As we have previously shown[7] the Fourier transform of the square of nuclear density in Eq. (2.10) is related to the antisymmetrized A-nucleon wave functions by

$$\begin{aligned} H(\vec{q}) &= A(A-1)(2\pi)^3 \int e^{-i\vec{q}\cdot\vec{r}} [\rho(\vec{r})]^2 d\vec{r} \\ &= \sum_j \sum_{i\neq j} \int d\vec{k}_1 d\vec{k}_2 \cdots d\vec{k}_A d\vec{\Delta}\, \delta(\vec{k}_1 + \vec{k}_2 + \cdots + \vec{k}_A + \vec{k})\, \psi^*_{-\vec{k}'}(\vec{k}_1, \vec{k}_2, \ldots, \vec{k}_i - \vec{\Delta}, \ldots, \vec{k}_j + \vec{\Delta} + \vec{q}, \ldots, \vec{k}_A) \\ &\quad \times \psi_{-\vec{k}}(\vec{k}_1, \vec{k}_2, \vec{k}_3, \ldots, \vec{k}_A) \ , \end{aligned} \tag{A3}$$

where $\vec{q} = \vec{k} - \vec{k}'$ and $\vec{\Delta} = \vec{k}_i - \vec{k}_i'$. The momenta $-\vec{k}$ and $-\vec{k}'$ represent the initial and final momentum of the target nucleus in the π-*nucleus* c.m. frame. The δ function in Eq. (A3) expresses the c.m. correlation of the A nucleons.

Equation (A3) can be evaluated analytically for harmonic oscillator wave functions. The result for ^{12}C with a same HO parameter R for both s- and p-shell nucleons is

$$\begin{aligned} H(\vec{q}) = \frac{(2\pi)^{3/2}}{R^3} &[A_0(A_0-1) + 2A_0A_1(\tfrac{1}{4})(1 - \tfrac{1}{12}q^2R^2) \\ &+ A_1(A_1-1)(\tfrac{5}{12})(1 - \tfrac{1}{6}q^2R^2 + \tfrac{1}{240}q^4R^4)] \\ &\times e^{-5q^2R^2/48} \ , \end{aligned} \tag{A4}$$

where $A_0 = 4$ and $A_1 = 8$. We note the relation $A_0(A_0-1) + 2A_0A_1 + A_1(A_1-1) = A(A-1)$ for $A = A_0 + A_1$. The generalization to different HO parameters for s- and p-shell nucleons is

$$\begin{aligned} H(\vec{q}) = \frac{(2\pi)^{3/2}}{R_0^3} &\Big[A_0(A_0-1)e^{-q^2R_0^2/8} + 2A_0A_1\left(\frac{\beta}{R_1}\right)^5 (\tfrac{1}{4} - \tfrac{1}{48}q^2\beta^2) e^{-q^2\beta^2/8} \\ &+ A_1(A_1-1)\frac{5R_0^3}{12R_1^3}(1 - \tfrac{1}{6}q^2R_1^2 + \tfrac{1}{240}q^4R_1^4) e^{-q^2R_1^2/8}\Big] e^{q^2\beta^2/48} \end{aligned} \tag{A5}$$

with

$$\beta^2 \equiv 2R_0^2R_1^2/(R_0^2 + R_1^2) \ . \tag{A6}$$

Here, with different oscillator parameters for the s and p shells, the c.m. correlation is only treated approximately. The approximation is, however, adequate since the values for R_0(=1.63 fm) is very close to that for R_1(=1.64 fm).

[1] R. H. Landau, S. C. Phatak, and F. Tabakin, Ann. Phys. (N.Y.) 78, 299 (1973); M. G. Piepho and G. E. Walker, Phys. Rev. C 9, 1352 (1974); L. S. Kisslinger and F. Tabakin, *ibid.* 9, 188 (1974); J. P. Dedonder, Nucl. Phys. A174, 251 (1971); A180, 472 (1972); R. Mach, *ibid.* A258, 513 (1976). For an alternate point of view, see G. E. Brown and W. Weise, Phys. Rep. 22, 279 (1975).

[2] R. H. Landau and A. W. Thomas, Phys. Lett. 61B, 361 (1976).

[3] L. C. Liu and C. M. Shakin, Phys. Rev. C 16, 1963 (1977).

[4] L. Celenza, L. C. Liu, and C. M. Shakin, Phys. Rev. C 11, 1593 (1975). 12, 721(E) (1975).

[5] L. Celenza, L. C. Liu, and C. M. Shakin, Phys. Rev. C 12, 1983 (1975). Improved versions of the calculations reported in this reference are to be found in Ref. 3.

[6] F. Lenz, in Proceedings of the Topical Meeting on Intermediate Energy Physics, March 31-April 10, 1976, Zuoz, Switzerland (unpublished), Vol. 2 [SIN Report (unpublished)].

[7] L. C. Liu and C. M. Shakin, Phys. Rev. C 16, 333 (1977). In this reference the parameters of the second-order optical potential for π^+-^{12}C scattering at 50 MeV were obtained. The data have since been modified and the parameters of the fit to the more recent data are given in the present work.

[8] R. R. Johnson, T. G. Masterson, K. L. Erdman, and A. W. Thomas, U. of British Columbia and TRIUMF report, April 1977 (unpublished).

[9] R. H. Landau and A. W. Thomas, TRIUMF report, May 1977 (unpublished).

[10] K. G. R. Doss, S. A. Dytman, and R. R. Silbar, Meson-Nuclear Physics-1976 (Carnegie-Mellon Conference), edited by P. D. Barnes, R. A. Eisenstein, and L. S. Kisslinger (AIP, New York, 1976), p. 344.

[11] L. S. Celenza, M. K. Liou, L. C. Liu, and C. M.

Shakin, Phys. Rev. C 10, 398 (1974). In this reference, the quantity W' under the integral of Eq. (12) should be correctly printed as $2W'-W$.
[12]L. Tauscher and W. Schneider, Z. Phys. 271, 409 (1974).
[13]K. M. Crowe, A. Fainberg, J. Miller, and A. S. L. Parsons, Phys. Rev. 180, 1349 (1965).
[14]F. Binon, P. Duteil, M. Gouanere, L. Hugon, J. Jansen, J. P. Lagnaux, H. Palevsky, J. P. Peigneux, M. Spighel, and J. P. Stroot, Phys. Rev. Lett. 35, 145 (1975); Nucl. Phys. B (to be published).
[15] S. A. Dytman *et al.*, Phys. Rev. Lett. 39, 53 (1977). This reference presents a modification of the 50 MeV π^+-^{12}C data previously reported by this group.
[16]F. Binon *et al.*, Nucl. Phys. B17, 168 (1970).
[17]D. J. Herndon, A. Barbaro-Galtieri, and A. H. Rosenfeld, UCRL Report No. UCRL-20030 πN (unpublished), p. 79.
[18]J. T. Londergan, K. W. McVoy, and E. J. Moniz, Ann. Phys. (N.Y.) 86, 147 (1974).
[19]M. Salomon, TRIUMF Report No. TRI-74-2 (unpublished).
[20]A large number of microscopic calculations of pion absorption have been presented in the literature. Most of the works were based on the quasideuteron model. See for the example: K. Brueckner, Phys. Rev. 98, 769 (1955); M. Ericson and T. E. O. Ericson, Ann. Phys. (N.Y.) 36, 323 (1966). More detailed analyses including off-shell effects may be found in Refs. 6 and 9, and in F. Hachenberg and H. J. Pirner, University of Heidelberg report (unpublished); F. Hachenberg, J. Hufner, and H. J. Pirner, Phys. Lett. 66B, 425 (1977).
[21]L. S. Celenza, L. C. Liu, and C. M. Shakin, Phys. Rev. C 11, 437 (1975).
[22]S. DeBenedetti, *Nuclear Interactions* (Wiley, New York, 1967), p. 188. The use of the realistic proton charge form factor was shown to be crucial in the understanding hadron-nucleus scattering at high energies. See L. C. Liu and C. M. Shakin, Phys. Rev. C 14, 1885 (1976).